ACI STRUCTURAL JOURNAL TECHNICAL PAPER

Title no. 100-S37

Seismic Performance of Hollow Bridge Columns

by Y. L. Mo, D. C. Wong, and K. Maekawa

Twenty-eight compression tests were carried out on concrete panels to determine the complete stress-strain relationship of the confined concrete in hollow bridge columns. Nine analytical models were used to analyze the test specimens. The test results were compared with the analytical results. Based on the comparison, the Muguruma et al. model was modified to accurately predict the stress-strain relationship of the confined concrete. The seismic performance of hollow bridge columns was further studied by reversed cyclic loading tests. The parameters of the test program were concrete compressive strength, configuration of lateral steel, and spacing of lateral steel. It was found that the modified Muguruma et al. model can be adopted in the moment-curvature analysis to properly predict the horizontal force-displacement relationship of hollow columns with acceptable accuracy.

Keywords: column; compressive strength; concrete; seismic; test.

INTRODUCTION

The high-speed rail project to improve Taiwan's transportation systems is an effort by the Taiwanese government to further the island's economic development. The planned route is 345 km long. The viaducts and bridges are approximately 207 km long. Hence, there are many bridge columns in the project. To maximize structural efficiency in terms of the strength-to-mass and stiffness-to-mass ratios and to reduce the mass contribution of the column to seismic response, it is desirable to use a hollow section for the columns. The configuration of lateral steel in the hollow columns studied in the past is shown in Fig. 1(a) to (g).[1-7] To consider both ductility and workability, the hollow section, as shown in Fig. 1(h), has been used in the bridge columns in the high-speed rail project of Taiwan.

During the past three decades, various studies on the confinement effects of lateral steel in columns have been conducted (Table 1). Kent and Park[8] proposed a stress-strain model consisting of a second-order parabola ascending branch and a straight line descending branch. In this model, the effects of confinement were reflected by adjusting the slope of the descending branch. Park et al.[16] revised the prototype model to introduce the increase in concrete strength caused by confinement. It was assumed that the confinement effect was proportional to the volumetric ratio and yield strength of confining reinforcement. Sheikh and Uzumeri[10,17] proposed a stress-strain model that reflects the confinement effect by adjusting the peak stress and a confinement effectiveness coefficient. The confinement effectiveness coefficient depends on the configuration of confining steel. The deterioration rate of the falling branch is similar to that in the model of Park et al.[16] Mander, Priestley, and Park[11] proposed a fractional expression to represent both the ascending and falling branches of the stress-strain curve. To evaluate the peak stress, a confinement effectiveness coefficient for circular, square, and wall-type sections was introduced based on a theory similar to Sheikh and Uzumeri.[10,17] Furthermore, a constitutive model involving a specified ultimate strength surface for multiaxial compressive stresses was applied in the model, which enabled development of a theoretical model without dependence on a statistical analysis of test results. This model was found to provide good predictions of test results.[12] Saatcioglu and Razvi[14] and Razvi and Saatcioglu[18] proposed a parabolic ascending branch, followed by a linear falling branch. The falling branch was a function of the strain corresponding to 85% of the peak stress. Many test data were evaluated to establish the parameters of this analytical model.[14,18] Muguruma et al.[19] proposed a model of

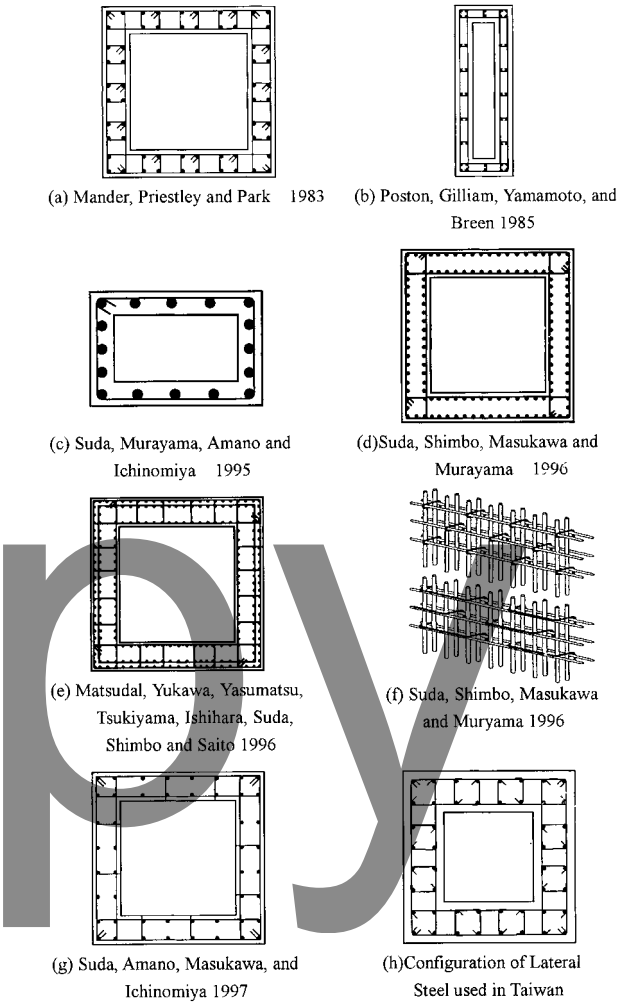

Fig. 1—Configuration of lateral steel in hollow columns.

ACI Structural Journal, V. 100, No. 3, May-June 2003.
MS No. 02-126 received April 4, 2002, and reviewed under Institute publication policies. Pertinent discussion including authors' closure, if any, will be published in the March-April 2004 *ACI Structural Journal* if the discussion is received by November 1, 2003.

ACI member **Y. L. Mo** *is a professor in the Department of Civil and Environmental Engineering, University of Houston, Houston, Tex. He received his PhD from the University of Hannover, Hannover, Germany, in 1982. He is a member of ACI Committees 335, Composite and Hybrid Structures; 369, Seismic Repair and Rehabilitation; 374, Performance-Based Seismic Design of Concrete Buildings; 444, Experimental Analysis for Concrete Structures; and Joint ACI-ASCE Committee 445, Shear and Torsion. His research interests include seismic performance of concrete structures.*

D. C. Wong *is an assistant professor in the Department of Architecture, Kao-Yuan Institute of Technology, Tainan, Taiwan. He received his PhD from National Cheng Kung University. His research interest includes structural concrete and engineering mechanics.*

K. Maekawa *is a professor in the Department of Civil Engineering, the University of Tokyo, Tokyo, Japan. He received his PhD in engineering from the University of Tokyo, 1985. His research interests include nonlinear structural mechanics and multi-scale analysis of cementitious composite for durability design.*

the stress-strain curve constructed by two second-order parabolas. The confinement effect was evaluated in terms of a confinement effectiveness coefficient. An evaluation method for the peak stress and the ultimate strain was proposed based on a statistical study of test results.[9] Fujii et al.[13] proposed a model consisting of a second-order parabola and a third-order curve for the ascending branch. A confinement effectiveness coefficient, based on the model by Park et al.[16] was proposed. The peak stress and the deterioration rate were expressed as a linear function of the confinement effectiveness coefficient, based on a regression analysis of test results. Hoshikuma et al.[15] proposed a model consisting of three parts, that is, an ascending branch, falling branch, and sustaining branch. The stress of concrete is represented by a higher-order function that satisfies the four boundary conditions. Recently, Sheikh and Khoury[20] proposed a performance-based approach for the design of confining steel in tied columns.

In this research, because of the following two reasons, the stress-strain relationship of confined concrete in hollow bridge columns was first studied by panel tests. 1) The effect of the configuration of lateral steel on the hollow columns, as shown in Fig. 1(h), has never been studied by tests. 2) It is not known that any of the existing stress-strain models of confined concrete are appropriate for the hollow sections, as shown in Fig. 1(h). It was found from the panel tests that the Muguruma et al. model of confined concrete can be modified to predict the stress-strain relationship of confined concrete in such columns more accurately. In addition, eight scaled hollow bridge columns were tested. Experimental parameters include axial loads ranging from 6 to 19% of column axial-load-carrying capacity based on concrete gross section, configuration of lateral steel, and concrete compressive strengths of 25 to 50 MPa. It was found that the modified Muguruma et al. model can be adopted in the moment-curvature analysis to properly predict horizontal force-displacement relationship of hollow columns. The comparison of analytical results with experimental data showed a good agreement.

RESEARCH SIGNIFICANCE

A configuration of lateral steel in hollow bridge columns is presented in this paper that is quite different from those studied in the past.[1-7] The stress-strain relationship of confined concrete by the proposed configuration was experimentally investigated. Based on the test results, an analytical model to predict the stress-strain relationship of confined concrete is proposed. The seismic performance of the hollow bridge columns is further studied by

Table 1—Summary of previous stress-strain models for confined concrete

Researcher	Stress-strain model for confined concrete			Applicable cross-sectional shape
	Ascending branch	Descending branch	Residual stress	
Kent and Park[8]	$f_c = f'_c\left[\frac{2\varepsilon}{0.002} - \left(\frac{\varepsilon}{0.002}\right)^2\right]$	$f_c = f'_c[1 - Z(\varepsilon - 0.002)]$	—	Square
Confined Kent and Park[8]	$f_c = f'_c\left[\frac{2\varepsilon}{0.002} - \left(\frac{\varepsilon}{0.002}\right)^2\right]$	$f_c = f'_c[1 - Z(\varepsilon - 0.002)]$	20% of f'_c	Square
Modified Kent and Park[8]	$f_c = Kf'_c\left[\frac{2\varepsilon}{0.002K} - \left(\frac{\varepsilon}{0.002K}\right)^2\right]$	$f_c = Kf'_c[1 - Z_m(\varepsilon - 0.002K)]$	20% of Kf'_c	Square
Muguruma et al.[9]	$f_c = E_c\varepsilon + \frac{f'_c - E_c\varepsilon_c}{\varepsilon_c^2}\varepsilon^2$ $f_c = \frac{f'_c - f_{cc}}{(\varepsilon_c - \varepsilon_{cc})^2}(\varepsilon - \varepsilon_{cc})^2 + f_{cc}$	$f_c = \frac{f_{cu} - f_{cc}}{\varepsilon_{cu} - \varepsilon_{cc}}(\varepsilon - \varepsilon_{cc}) + f_{cc}$	—	Circle Square
Sheikh and Uzumeri[10]	$f_c = f_{cc}\left[\frac{2\varepsilon}{\varepsilon_{s1}} - \left(\frac{\varepsilon}{\varepsilon_{s1}}\right)^2\right]$	$f_c = f_{cc}[1 - Z(\varepsilon - \varepsilon_{s2})]$	30% of f_{cc}	Square
Mander, Priestley, and Park[11,12]	$f_c = \frac{f_{cc}xr}{r - 1 + 1x^r}$	$f_c = \frac{f_{cc}xr}{r - 1 + 1x^r}$	—	Circle Square Wall-type
Fujii et al.[13]	$f_c = E_c\varepsilon + \frac{f_{cc} - E_c\varepsilon_c}{\varepsilon_c^2}\varepsilon^2$ $f_c = \frac{f'_c - f_{cc}}{(\varepsilon_c - \varepsilon_{cc})^3}(\varepsilon - \varepsilon_{cc})^3 + f_{cc}$	$f_c = f_{cc} - \theta(\varepsilon - \varepsilon_{cc})$	20% of f_{cc}	Circle Square
Saatcioglu and Razvi[14]	$f_c = f_{cc}\left[2\left(\frac{\varepsilon}{\varepsilon_{cc}}\right) - \left(\frac{\varepsilon}{\varepsilon_{s1}}\right)^2\right]^{1/(1+2K)}$	$f_c = f_{cc}\frac{0.15f_{cc}}{(\varepsilon_{85} - \varepsilon_{cc})}(\varepsilon - \varepsilon_{cc})$	20% of f_{cc}	Circle Square Wall-type
Hoshikuma et al.[15]	$f_c = E_c\varepsilon\left[1 - \frac{1}{n}\left(\frac{\varepsilon}{\varepsilon_{cc}}\right)^{n-1}\right]$	$f_c = f_{cc} - E_{des}(\varepsilon - \varepsilon_{cc})$	50% of f_{cc}	Circle Square

eight test columns. The effect of the concrete compressive strength, configuration type of lateral steel, and spacing of lateral steel on the seismic performance of hollow bridge columns was investigated.

Analytical model

Stress-strain relationship of concrete—As discussed later in this paper, nine stress-strain models of confined concrete were checked by panel tests. It was found that the Muguruma et al. model can be modified to predict the stress-strain relationship of confined concrete in hollow bridge columns.

Stress-strain relationship of longitudinal reinforcing bars

The stress-strain curve of a reinforcing bar in concrete relates the average stress to the average strain of a large length of reinforcing bar crossing several cracks, whereas the stress-strain curve of a bare reinforcing bar relates the stress to the strain at a local point. Therefore, the bilinear model of the average stress-strain relationship of reinforcing bars embedded in concrete suggested by Hsu[21] was used to determine the stress-strain relationship of reinforcing bars. The expressions are as follows

If

$$f_s \le f_y' \ , \ f_s = E_s\varepsilon_s \tag{1}$$

If

$$f_s > f_y' \ , \ f_s = (0.91 - 2B)f_y + (0.02 + 0.25B)E_s\varepsilon_s \tag{2}$$

where

$$f_y' = (0.93 - 2B)f_y \tag{3}$$

$$B = \frac{1}{\rho}\left(\frac{f_{cr}}{f_y}\right)^{1.5} \tag{4}$$

$$\rho = \frac{A_s}{A_g} \tag{5}$$

f_s = reinforcing bar stress;
f_y = yield stress of bare reinforcing bars;
E_s = modulus of elasticity of reinforcing bars;
ε_s = strain of reinforcing bars;
A_s = area of concrete section; and
f_{cr} = tensile cracking strength of concrete.

Moment-curvature relationship

According to the assumption that plane sections before bending remain plane after bending, the moment-curvature relationship of cross sections of hollow columns can be determined when the constitutive laws of concrete and steel mentioned previously and the equilibrium conditions of cross section are used. When the moment curvature relationship is obtained, the force-displacement relationship can be determined by the moment area method with the moment diagram of the column.

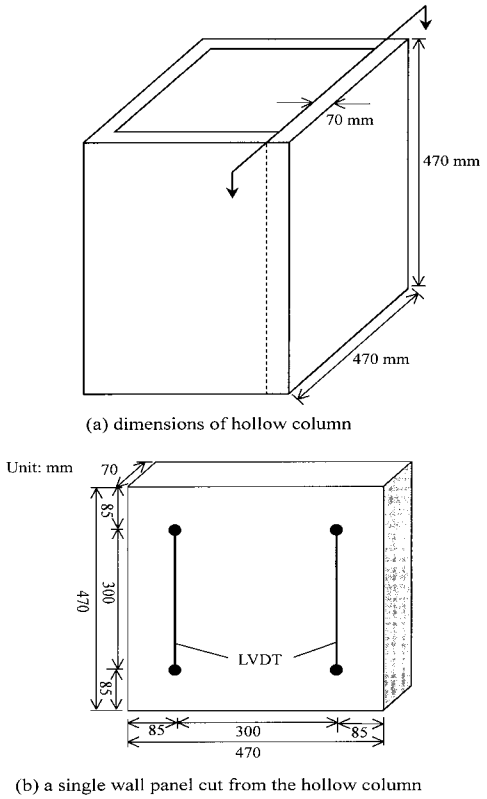

Fig. 2—Dimensions of specimens.

EXPERIMENTAL PROGRAM

Panel tests

Specimens—Fig. 2(a) indicates the dimensions of the hollow columns. When a single wall is cut from the hollow column, it is shown in Fig 2(b). Note that no concrete cover is considered in Fig. 2, that is, only confined concrete was studied. Three types of configurations of lateral steel, shown in Fig. 3, were tested, namely, Types A, B, and C. Type B is often employed in bridge engineering in Taiwan. As shown in Table 2, 28 specimens have been designed for compression tests. N and H in the first character of designation stand for normal and higher-strength concrete, respectively. A, B, and C in the second character of designation specify the configuration of lateral steel with Types A, B, and C, respectively, and 0 means pure concrete only. Three and 4 in the third character of designation represent the spacings of lateral steel of 30 and 40 mm, respectively. Because each case has two specimens, the last character of 1 and 2 means Specimens 1 and 2, respectively. It should be noted that the spacings of lateral steel of both 30 and 40 mm are satisfied with the requirement of the ACI Code.[22] When the following equation suggested by Priestley, Seible, and Calvi[23] was used, however,

$$s \le \left[3 + 6\left(\frac{f_u}{f_{y\ell}} - 1\right)\right]d_{b\ell} \tag{6}$$

where
s = spacing of lateral steel;
f_u = ultimate strength of longitudinal reinforcing bars;
$f_{y\ell}$ = yield stress of longitudinal reinforcing bars; and
$d_{b\ell}$ = diameter of longitudinal reinforcing bars.

it was found that the spacing should not be greater than 33 mm. With regard to the lateral steel, the test specimens were satisfied with the requirements of both the ACI code[22]

Table 2—Results of panel tests

Specimen no.	f_c', MPa	Maximum stress, MPa	Maximum strain	Ultimate stress, MPa	Ultimate strain
N001	22	22.75	0.0025	21.97	0.0028
N002	22	19.98	0.0016	15.98	0.0026
NA31	22	34.00	0.0050	27.20	0.0085
NA32	22	34.81	0.0065	27.85	0.0105
NA41	22	32.73	0.0041	26.18	0.0078
NA42	22	33.79	0.0037	27.03	0.0060
NB31	22	35.33	0.0066	28.27	0.0101
NB32	22	31.79	0.0057	25.43	0.0114
NB41	22	31.96	0.0048	25.57	0.0086
NB42	22	26.20	0.0045	20.96	0.0078
NC31	22	36.22	0.0061	28.97	0.0106
NC32	22	29.34	0.0078	23.47	0.0123
NC41	22	35.48	0.0057	28.38	0.0096
NC42	22	34.37	0.0061	27.50	0.0087
H001	41	39.29	0.0021	31.43	0.0031
H002	41	34.37	0.0017	27.50	0.0030
HA31	41	50.38	0.0035	42.98	0.0048
HA32	41	49.39	0.0023	36.31	0.0035
HA41	41	52.94	0.0026	42.35	0.0045
HA42	41	52.67	0.0023	42.14	0.0033
HB31	41	55.62	0.0028	44.49	0.0048
HB32	41	55.12	0.0029	44.10	0.0045
HB41	41	54.87	0.0036	43.90	0.0063
HB42	41	47.11	0.0019	37.69	0.0031
HC31	41	55.86	0.0036	44.69	0.0037
HC32	41	52.27	0.0050	49.95	0.0051
HC41	41	56.51	0.0038	45.21	0.0059
HC42	41	48.37	0.0019	38.69	0.0028

$$A_{sh} \geq 0.3 s h_c \frac{f_c'}{f_{yh}} \left(\frac{A_g}{A_{ch}} - 1 \right) \quad (7)$$

and

$$A_{sh} \geq 0.09 s h_c \frac{f_c'}{f_{yh}} \quad (8)$$

where

A_{sh} = total area of lateral steel within spacing s and perpendicular to dimension h_c;
s = spacing of lateral steel;
h_c = dimension of column core measured center-to-center of confining reinforcement;
A_{ch} = area of member measured out-to-out of lateral steel;
A_g = gross area of section;
f_c' = concrete compressive strength; and
f_{yh} = yield stress of lateral steel

and the equation suggested by Priestley, Seible, and Calvi[23]

$$A_{sh} = 0.12 s h_c \frac{f_c'}{f_{y\ell}} \left(0.5 + \frac{1.25P}{f_c' A_g} \right) + 0.13(\rho_\ell - 0.01) \quad (9)$$

where

P = axial force; and
ρ_ℓ = reinforcement ratio of longitudinal bars.

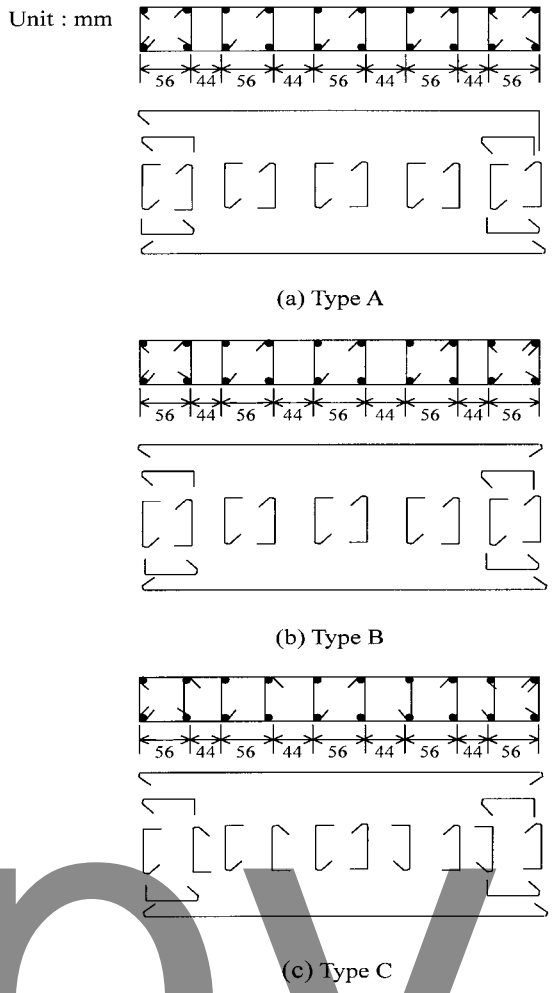

Fig. 3—Configuration of lateral steel: reinforcing bars f = 6 mm, and lateral steel f = 4 mm.

Note that the diameters of longitudinal and lateral bars were 6 and 4 mm, respectively.

Materials

The concrete was supplied by a local ready-mix concrete plant with two kinds of compressive strengths, namely, 22 and 41 MPa. The measured concrete strength values, also shown in Table 2, were obtained using 150 x 300 mm cylinders at the test age, which was about 30 days after casting. The bars with the diameters of 6 and 4 mm had yield strengths of 459.5 and 400.0 MPa, respectively.

Test setup

The specimens were tested under a universal compression machine that has a capacity of 500 tons. A thick steel plate was attached to each of the tops and bottoms of the specimens. At the bottom of the thick steel plate, a load cell was connected to measure the axial force. In each face of the specimen there were two linear variable differential transducers (LVDTs), whose locations are shown in Fig. 2. It should be noted that the LVDT's gage length of 300 mm was not too close to the loading plates because the panels did not fail in the regions of loading plates. Therefore, the test results were not affected by the loading plates. The axial force was monotonically increased until the maximum force of the specimen was reached. After the peak force, tests were controlled by displacement.

Table 3—Properties of specimens

Specimen no.	f'_c, N/mm^2	P, kN	$P/f'_c A_g$	Yielding stress, N/mm^2	
				Reinforcing bar	Stirrups
NA4	30.1	900	0.19	459.5	400.0
NB4	30.1	450	0.09		
NA8	24.6	450	0.11		
NB8	24.6	450	0.11		
HA4	49.9	900	0.11		
HB4	49.9	450	0.06		
HA8	35.8	450	0.08		
HB8	35.8	450	0.08		

Note: f'_c = concrete compressive strength; P = axial force; and A_g = area of cross section.

Hollow column tests

Eight reinforced concrete hollow columns were tested under a constant axial force varying from 0.06 to 0.19$f'_c A_g$ and a cyclically reversed horizontal load. The parameters for the specimens were concrete compressive strength, spacing of lateral steel, and configuration of confining steel. Table 3 shows these parameters used in the specimens. The following properties obtained from the material tests were used later in the analytical predictions: yield stress of longitudinal reinforcing bars f_y = 459.5 (N/mm^2), ultimate strength of longitudinal reinforcing bars f_y = 663.0 (N/mm^2), ultimate strain of longitudinal reinforcing bars ε_u = 0.023, yield stress of lateral steel f_{yh} = 400.0 (N/mm^2), modulus of elasticity of steel $E_s = 2.1 \times 10^5$ (N/mm^2), and the concrete strength is shown in Table 3.

Specimens

The column and footing of each specimen were designed according to the ACI 318-02 seismic provisions,[22] and there were two kinds of configurations of confining steel, namely Types A and B, as shown in Fig. 4. Figure 4 also indicates the dimensions of the cross section of the specimens. Note that Type B has been used currently in bridge design in Taiwan, and Type A has never been used but will possibly be adopted by engineers. One of the purposes of this study was to verify the confining effect that resulted from these two types. The cross section of each specimen was 500 x 500 mm; the length and wall thickness of the hollow column were 2 and 100 mm, respectively. The first character of the specimen name stands for the concrete compressive strength (Normal or Higher); the second character stands for the configuration type (A or B); and the last character represents the spacing of the confining steel (40 or 80 mm). In this paper, the spacing of the confining steel satisfies the requirement specified in the ACI Code,[22] but it didn't satisfy the requirements suggested by Priestley, Seible, and Calvi[23] in which the spacing needs to be less than six times the diameter of longitudinal reinforcing bars. It should be noted that the compression force and bending moment of each of all eight specimens were plotted in the interaction diagram (Fig. 5). It can be seen from Fig. 5 that all eight specimens were tension-controlled columns.

Test setup and loading sequence

A schematic drawing of the test setup is shown in Fig. 6. The specimen was mounted vertically with the bottom of the reinforced concrete foundation being held by a steel foundation, and the end of the column was held by a hydraulic jack to provide a constant axial force. Under the hydraulic jack, the column was held by an actuator that was horizontally mounted

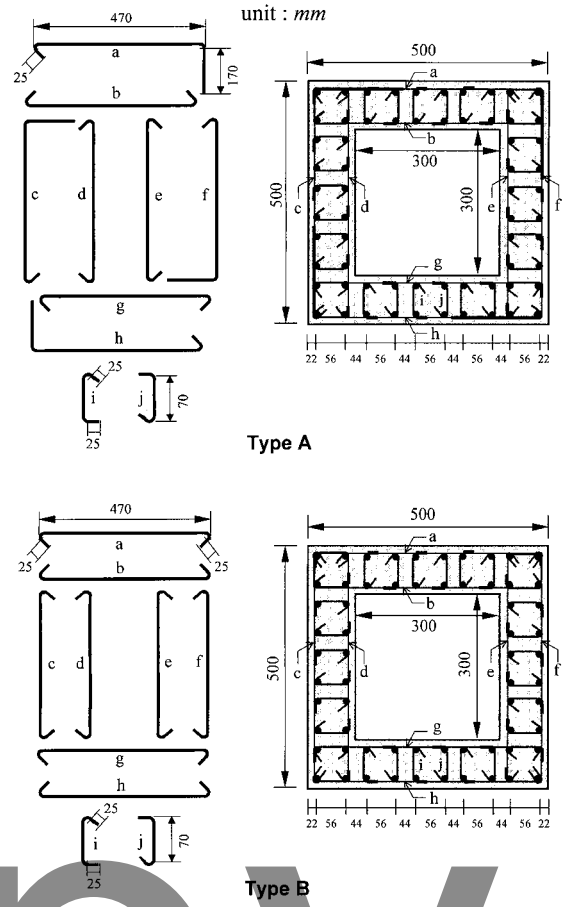

Fig. 4—Configurations of lateral steel (reinforcing bars f = 6 mm, lateral steel f = 4 mm).

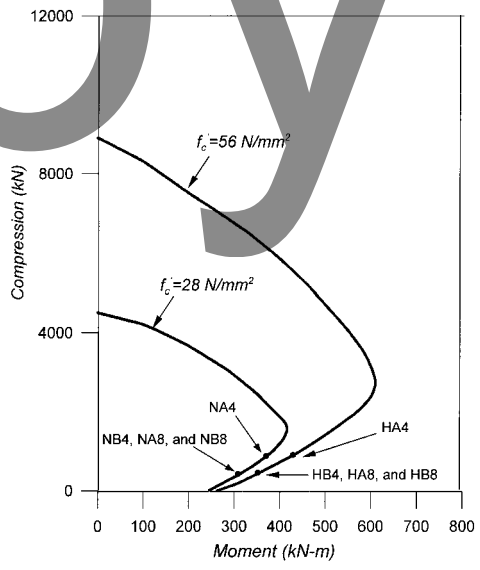

Fig. 5—Interaction diagram of compression and moment.

to a reaction wall. The actuator had a capacity of 500 kN and was capable of moving the column 150 mm in both positive and negative directions. A displacement of 150 mm corresponds to a column drift (ratio of horizontal displacement to column height) of 7.5%. Each specimen was instrumented with load cell, displacement transducers, and strain gages to monitor the applied displacements and corresponding loads as well as the resulting strains and relative deformations.

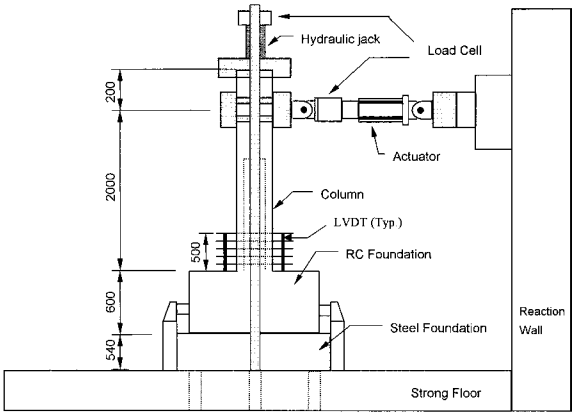

Fig. 6—Test setup (unit:mm).

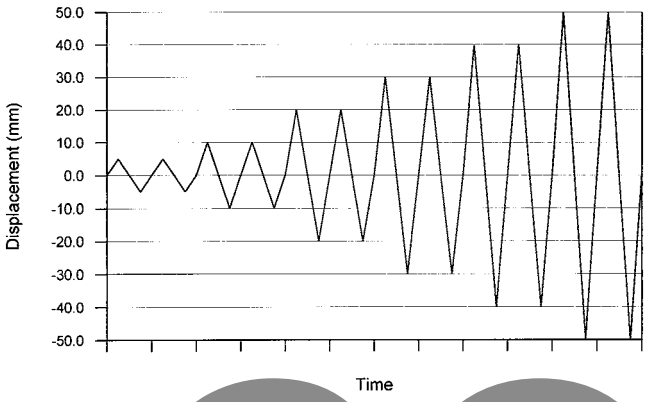

Fig. 7—Loading history.

The specimens were tested under displacement control, following a predetermined displacement history defined in terms of column drift percentage. The displacement routine, shown in Fig. 7, consists of cycles with column drift ratios up to 2.5%. The displacement cycles were repeated to measure the strength degradation.

EXPERIMENTAL RESULTS

Panel tests

Failure mode—Three failure modes were observed, namely, concrete splitting, concrete crushing, and reinforcing bar buckling. The experimental observations described as follows were based on the failure mode.

Concrete splitting—The failure mode of the specimens with pure concrete (N001, N002, H001, and H002) was concrete splitting. Before the maximum compression force was reached, there had been only some minor cracks. Soon after the maximum compression force, there was an enormous sound of explosion, and serious cracks occurred suddenly from the top to the bottom. Finally, the specimens split away (Fig. 8(a)).

Concrete crushing—Before the maximum compression force was reached, there had been some minor cracks. Right after the maximum compression force, cracks increased with increasing displacements. Finally, serious cracks increased suddenly and the concrete close to the middle of the specimen crushed (Fig. 8(b)). Most of the specimens (Table 2) had this kind of failure mode.

Reinforcing bar buckling—Similar to the failure modes of concrete splitting and concrete crushing, before the maximum compression force was reached, there had been some minor cracks. After the maximum compression force, however, cracks increased with increasing displacements and confining steel expanded outward. Finally, reinforcing bars buckled locally (Fig. 8(c)). Only Specimens HB42 and HC42 had this kind of failure mode.

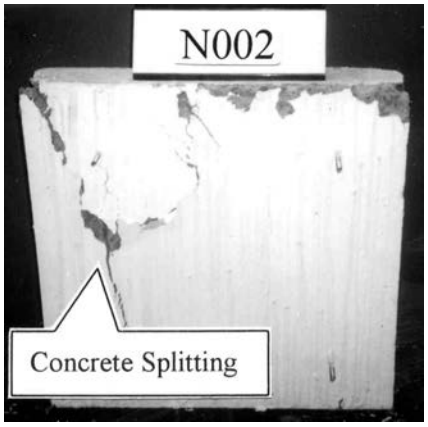

(a)

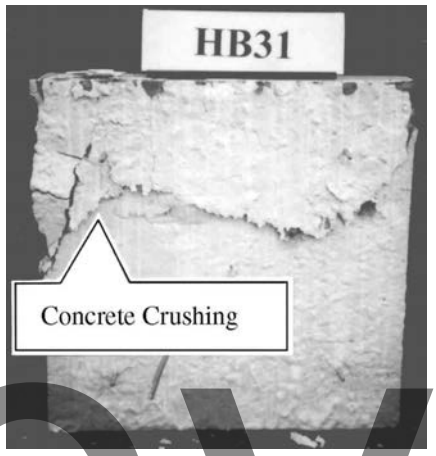

(b)

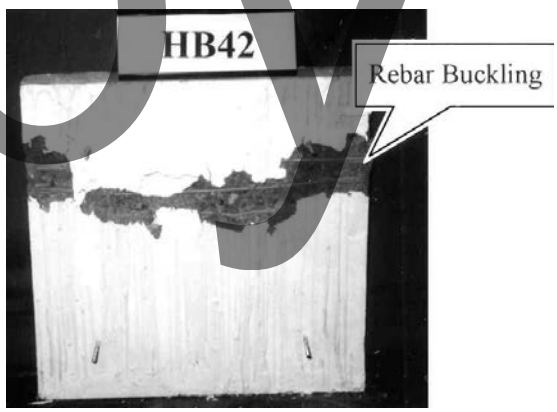

(c)

Fig. 8—Failure modes of panels: (a) concrete splitting; (b) concrete crushing; and (c) reinforcing bar buckling.

Effect of concrete strength

It can be seen from Fig. 9 that the specimens with higher concrete strength have greater slope of elasticity and maximum compression force than those with normal concrete strength. In other words, the stiffness and maximum stress of the specimens with higher concrete strength are greater.

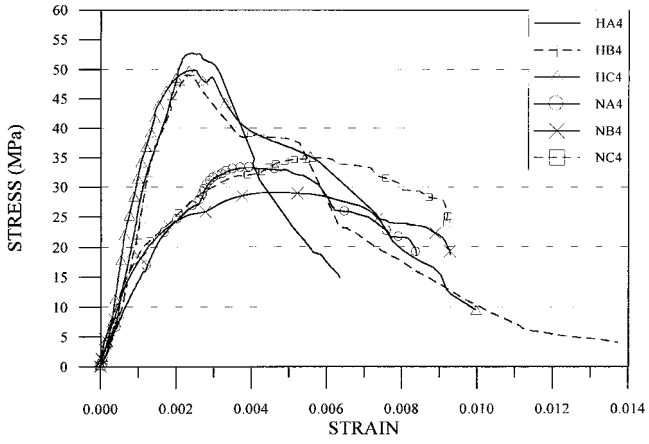

Fig. 9—Effect of concrete strength on stress-strain relationships.

It can also be seen from Table 2 that for the specimens with pure concrete, the ultimate strain of the specimens with higher strength is slightly greater than that with normal strength. For the specimens with confining steel, however, the ultimate strain of the specimens with normal strength is approximately twice as large as that with higher strength. Note that the ultimate strain is defined as the strain corresponding to 80% of the maximum stress in the descending branch. In other words, confined specimens with normal strength had better ductility. By observation during testing, it could also be found that the concrete spalling of the specimens with higher concrete strength happened easier; moreover, cracks grew faster.

Effect of configuration of lateral steel

It can be seen from Fig. 10 that the stiffness, maximum stress, and ductility of Types A, B, and C are very close as long as the concrete strength and the spacing of confining steel are the same. In other words, the effect of configuration of lateral steel used in this study on the stress-strain relationship of confined concrete is small and negligible. The stress-strain relationship of each of both pure concrete panel and standard 150 x 300 mm cylinder is also shown in Fig. 10 for comparison. It can be seen from Fig. 10 that the slope of the stress-strain relationship of cylinders is smaller than that of the remaining curves. The reason may result from different gage length. The gage length for cylinders is 100 mm; however, it is 300 mm for all panels. The shorter gage length results in smaller slope.

Effect of spacing of lateral steel

In this study, there were two different spacings, namely, 30 and 40 mm. It can be seen from Fig. 11 and Table 2 that for the specimens with normal strength concrete and same confining condition, smaller spacing of confining steel (30 mm) had better confinement effect (Fig. 11); hence, their ductilities and strengths were greater than those with larger spacing (40 mm). For the specimens with higher-strength concrete and same confining condition, however, different spacing (30 or 40 mm) gave no obvious deviation in ductility. In contrast, smaller spacing provided somewhat greater strength than larger spacing. It should be noted that no reinforcing bar buckling occurred in the specimens with 30 mm spacing of confining steel, and reinforcing bar buckling occurred in some specimens with 40 mm spacing of confining steel. In other words, the spacing requirement specified in the ACI Code cannot be employed for concrete strength used in this

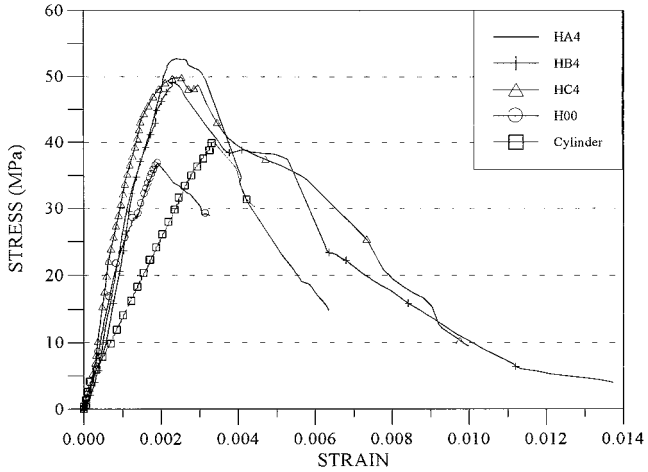

Fig. 10—Effect of configuration of lateral steel for specimens with higher-strength concrete.

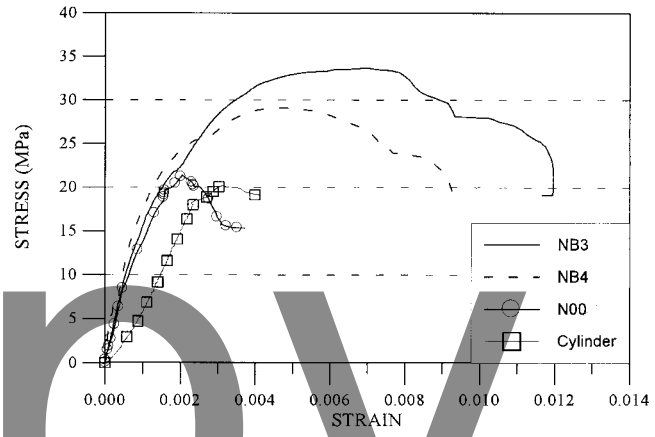

Fig. 11—Effect of spacing of lateral steel for specimens with normal-strength concrete.

study. In contrast, the equation suggested by Priestley, Seible, and Calvi[23] for the spacing of lateral steel can well be employed. Similar to Fig. 10, the stress-strain relationships of both pure concrete panels and standard 150 x 300 mm cylinder are also shown in Fig. 11 for comparison.

Comparison with analytical models

Figure 12 indicates a comparison of test data with analytical results for Specimen HC4. It can be seen from Fig. 12 that the prediction from the unconfined Kent and Park model is very different from the test results and the remaining eight confined models, and the experimental stress-strain relationship after the maximum stress descends faster than those predicted by the eight analytical models.

After careful examination, it was found that the Muguruma et al. model can easier be modified to predict the stress-strain relationship of confined concrete tested in this study. The modified Muguruma et al. model is proposed as follows (Fig. 13).

In the region of Curve AB

$$f_c = E_c\varepsilon + \frac{(f_c' - E_c\varepsilon_c)}{\varepsilon_c^2} \cdot \varepsilon^2 \qquad (10)$$

In the region of Curve BC

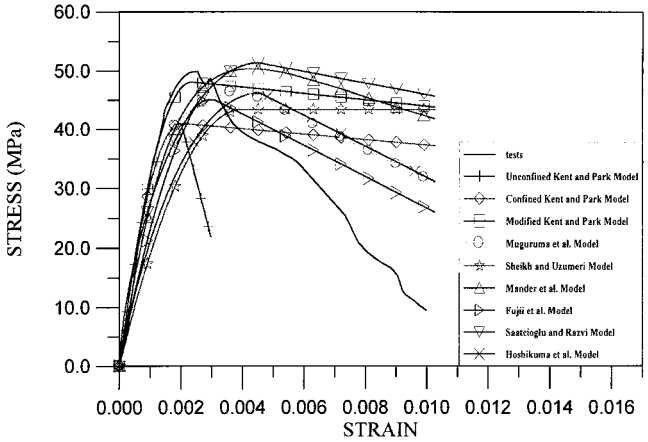

Fig. 12—Comparison of test results with nine analytical models for Specimen HC4.

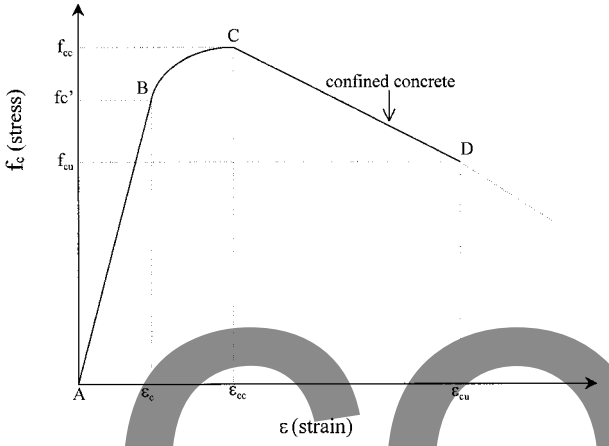

Fig. 13—Stress-strain curve of modified Muguruma et al. model.

$$f_c = \frac{(f_c' - f_{cc})}{(\varepsilon_c - \varepsilon_{cc})^2}(\varepsilon_c - \varepsilon_{cc})^2 + f_{cc} \quad (11)$$

In the region of Curve CD

$$f_c = \frac{f_{cu} - f_{cc}}{\varepsilon_{cu} - \varepsilon_{cc}}(\varepsilon_c - \varepsilon_{cc})^2 + f_{cc} \quad (12)$$

where

$$f_{cc} = (1 + 83C_c)f_c' \quad (13)$$

$$\varepsilon_{cc} = \left(1 + 450\left(1.85 - \frac{f_c'}{270}\right)C_c\right)\varepsilon_c \quad (14)$$

$$f_{cu} = \frac{2(A_o - f_{cc}\varepsilon_{cc})}{\varepsilon_{cu} + \varepsilon_{cc}} + f_{cc} \quad (15)$$

$$\varepsilon_{cu} = \left(1 + 450\left(0.74 - \frac{f_c'}{1230}\right)C_c\right)\varepsilon_u \quad (16)$$

$$C_u = \rho_s \frac{\sqrt{f_{yh}}}{f_c'}\left(1 - \frac{S}{(B_c + D_c)}\right) \quad (17)$$

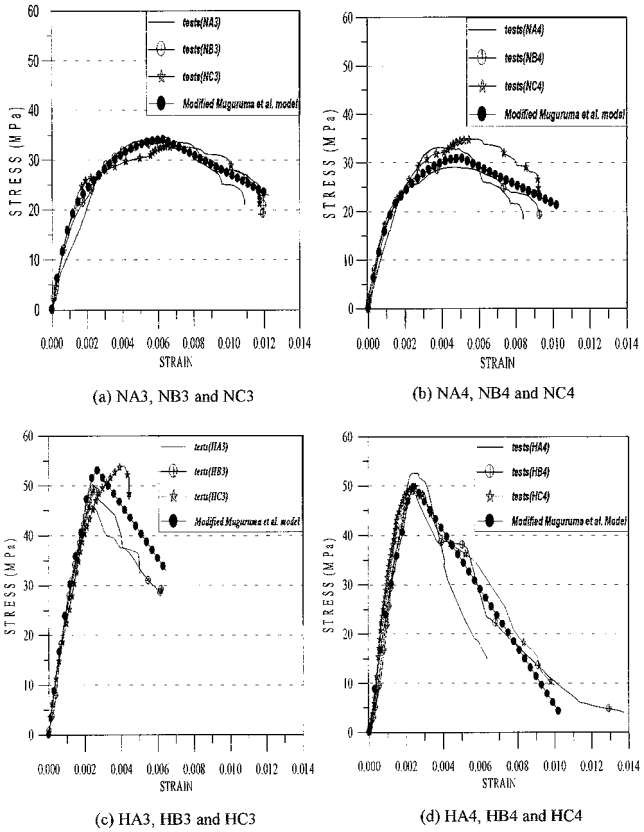

Fig. 14—Comparison of panel test results with modified Muguruma et al. model.

$$A_o = \frac{E_c\varepsilon_c^2}{6} + \frac{f_c'\varepsilon_{cc}}{3} + \frac{2f_{cc}}{3}(\varepsilon_{cc} - \varepsilon_c) \quad (18)$$

$$E_c = 4730\sqrt{f_c'}\ (\text{N/mm}^2) \quad (19)$$

Figure 14 indicates the comparison of the modified Muguruma et al. model with the test results for all specimens. It can be seen from Fig. 14 that the stress-strain relationship of confined concrete predicted by the modified Muguruma et al. model is in good agreement with the test results.

Hollow column tests

General observations—All eight hollow columns developed stable responses up to certain displacement ductility levels ranging from 3.7 to 7.2. Flexural cracks perpendicular to the column axis developed first in regions close to the bottom end of the columns. The flexural cracks became inclined and extended into the web zone of the columns due to the influence of shear, typically at a stage exceeding the first yield of longitudinal reinforcing bars. At later stages of loading, typically at displacement ductility levels of 2 and 3, independent shear cracks started to occur. Plastic hinges were fully formed at the bottom end of the columns, which contributed to the development of ductility. Although all eight specimens developed the estimated flexural strength, their ultimate performances and the ductility levels achieved were different for different testing conditions. As shown in Fig. 15, the ultimate failure modes for all eight columns were developed according to either of the following two scenarios.

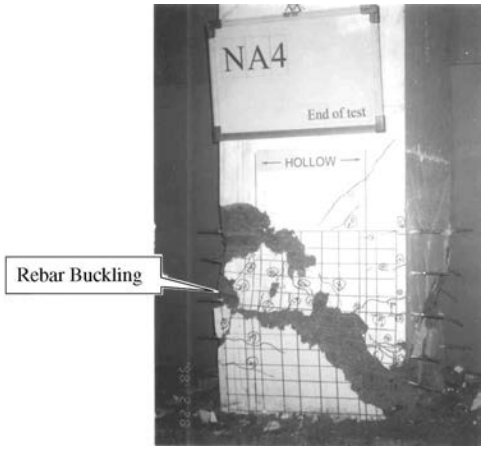

(a)

(b)

Fig. 15—Failure modes of hollow bridge columns: (a) reinforcing bar buckling; and (b) reinforcing bar rupture.

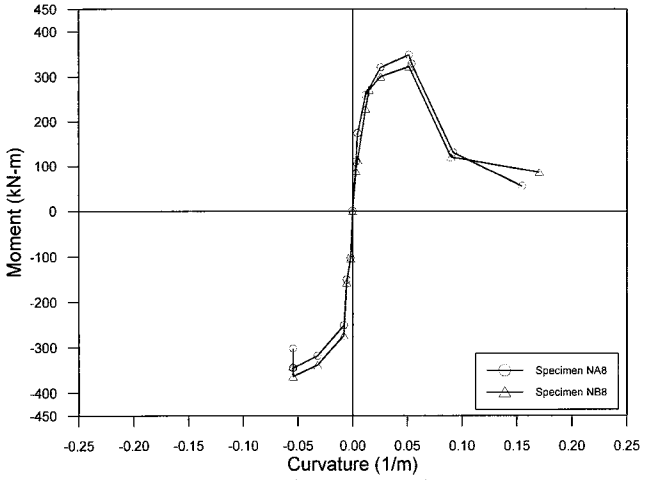

(a) Specimens NA8 and NB8

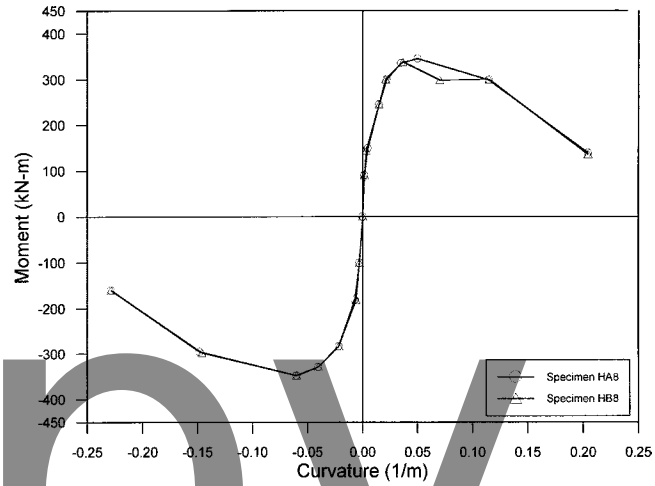

(b) Specimens HA8 and HB8

Fig. 16—Effect of configuration of lateral steel on moment-curvature curves.

Reinforcing bar buckling failure—Specimen NA4 was reinforced with 64 No. 2 (ϕ = 6 mm) longitudinal reinforcing bars and lateral ties of 4 mm diameter at a 40 mm center-to-center spacing, and was under an axial force of $0.19f'_cA_g$. The lateral reinforcement was sufficient for both shear strength and confinement based on current code provisions.[22] The specimen developed a displacement ductility factor of μ = 3.7; however, it lost its capacity upon the loading reversals at μ = 3.7 due to longitudinal reinforcing bar buckling followed by shear failure, as shown in Fig. 15(a).

Reinforcing bar rupture failure—The remaining seven specimens had the same longitudinal reinforcing bar and lateral ties as specimen NA4. The center-to-center spacing of lateral ties, however, were 40 or 80 mm. Because these specimens were subjected to lower axial forces ranging from 0.06 to $0.11f'_cA_g$, they developed displacement ductility factors from 5.6 to 7.2. The ultimate performances for these specimens were dominated by load-carrying capacity due to the rupture of tension longitudinal reinforcing bars at the bottom end of the columns, as shown in Fig. 15(b).

Effect of configuration of lateral steel

Figure 16 illustrates the effect of configuration of lateral steel on the moment-curvature curve. The moment was obtained using the horizontal force multiplied by the moment arm (distance from the actuator centerline to the top of footing). The curvature was determined by the measured displacement difference at the right and left surfaces of concrete in the plastic hinge region using LVDTs (Fig. 6) divided by the distance between the two displacement measurements. It can be seen from Fig. 16(a) that Specimen NA8 provided the performance similar to Specimen NB8. When Specimen HA8 was compared to Specimen HB8, the same conclusion could be made (Fig. 16(b)). In other words, the configuration of Type B can be replaced with that of Type A without reducing the seismic performance.

Effect of spacing of confining steel

Figure 17 illustrates the effect of spacing of confining steel on the moment-curvature curve. It can be seen from Fig. 17(a) that strength deterioration after the peak moment was apparent, when the spacing of confining steel increased for normal strength concrete, that is (NB8 versus NB4). This phenomenon, however, was not obvious for higher-strength concrete, as shown in Fig. 17(b). The reasons for this were that the ultimate strain of the used longitudinal reinforcing bars was small and the spalling of concrete did not occur at the ultimate state.

Effect of concrete compressive strength

Figure 18 illustrates the effect of concrete compressive strength on the moment-curvature curve. It can be seen from Fig. 18 that strength deterioration after the peak moment was

Table 4—Results of hollow column tests

Specimen no.	Yielding displacement, mm			Yielding force, kN			Ultimate displacement, mm			Maximum force, kN			Ductility factor			Energy dissipation, kN-mm	Failure mode
	+	–	Average	+	–	Average	+	–	Average	+	–	Average	+	–	Average		
NA4	10.6	10.9	10.8	100.2	100.6	100.4	38.5	41.5	40.0	180.0	176.0	178.0	3.6	3.8	3.7	22,744.0	Reinforcing bar buckled
NB4	6.2	7.7	7.0	75.0	82.1	78.6	44.6	41.5	43.1	171.0	170.0	170.5	7.2	5.4	6.3	15,534	Reinforcing bar broken
NA8	5.4	8.8	7.1	80.4	89.0	84.7	45.8	42.3	44.1	173.0	172.0	172.5	8.5	4.8	6.6	16,114	
NB8	6.5	6.5	6.5	70.0	78.9	74.5	40.0	41.5	40.8	172.0	172.0	172.0	6.2	6.4	6.3	17,878	
HA4	6.9	6.9	6.9	114.3	94.6	104.5	39.9	37.7	38.8	215.0	215.0	215.0	5.8	5.5	5.6	21,575	
HB4	5.4	5.8	5.6	75.7	61.4	68.6	35.8	43.8	39.8	177.0	177.0	177.0	6.6	7.6	7.1	19,108	
HA8	4.8	6.9	5.9	86.4	86.0	86.2	40.5	40.8	40.7	173.0	174.0	173.5	8.4	5.9	7.2	18,122	
HB8	5.4	6.8	6.1	73.9	80.4	77.2	41.5	43.8	42.7	177.0	174.0	175.5	7.7	6.4	7.1	17,057	

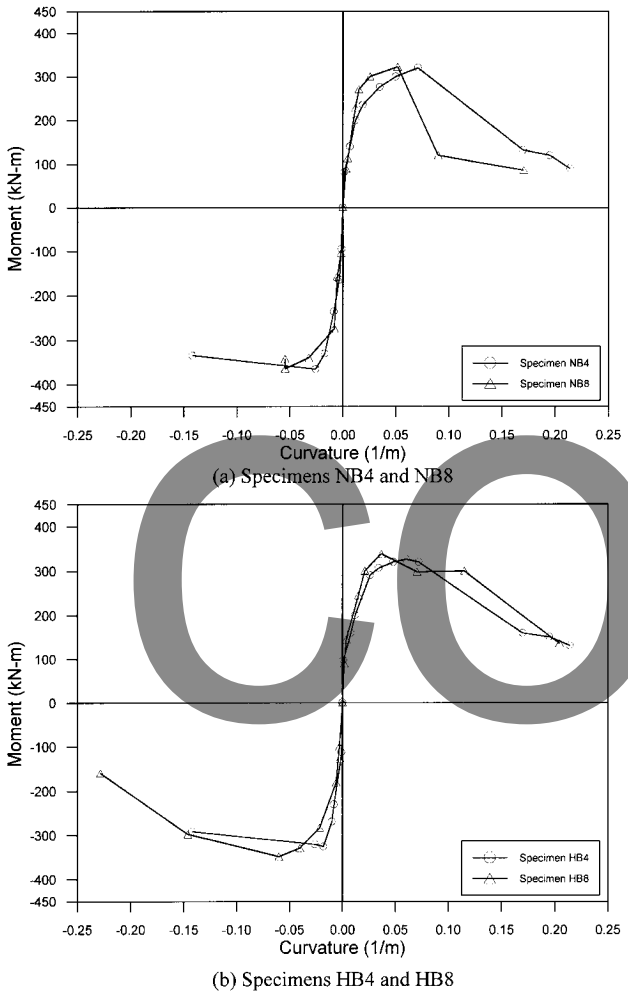

(a) Specimens NB4 and NB8

(b) Specimens HB4 and HB8

Fig. 17—Effect of spacing of confining reinforcement on moment-curvature curves.

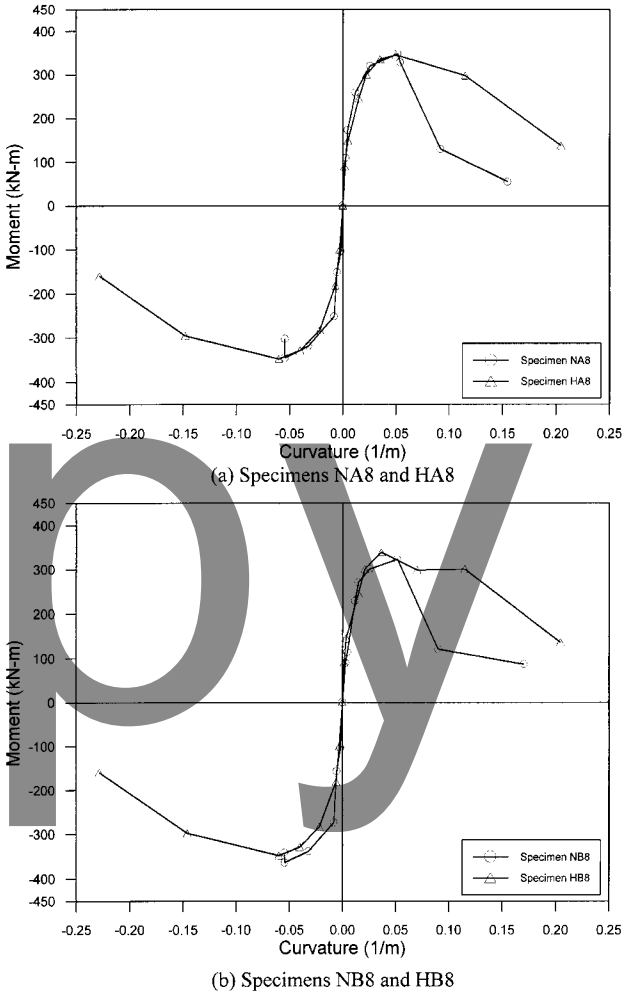

(a) Specimens NA8 and HA8

(b) Specimens NB8 and HB8

Fig. 18—Effect of concrete compressive strength on moment-curvature curves.

apparent for both Types A and B configuration of lateral steel. It was also clear that the dissipated energy for higher-strength concrete was greater than that for normalstrength concrete.

Ductility factor and dissipated energy

The ductility factor is defined as the displacement at 80% of the maximum horizontal force in the descending portion divided by the displacement at the occurrence of the first yield of longitudinal steel. The dissipated energy was determined by integrating the areas bounded by all the hysteretic loops. Table 4 gives the experimental results of the ductility factor and dissipated energy for all specimens. It can be seen from Table 4 that the range of ductility factor for all eight specimens was from 3.7 to 7.2. Although both types of columns were heavily confined by ties, the behavior of hollow bridge columns was not as ductile as the rectangular solid columns. The following reasons may have been involved: 1) the confined area in hollow bridge columns is relatively small when compared to the rectangular solid columns; and 2) the hollow bridge columns without concrete in the core expedite the failure of the concrete. Also, it should be noted that specimens with higher-strength concrete had greater ductility when the failure mode was rupture of longitudinal steel.

Table 5—Comparison of analytical results with test data

Specimen no.	Yielding displacement, mm		Yielding force, kN		Ultimate displacement, mm		Maximum force, kN		Ductility factor	
	Modified Muguruma et al. model	Test	Modified Muguruma et al. model	Test	Modified Muguruma et al. model	Test	Modified Muguruma et al. model	Test	Modified Muguruma et al. model	Test
NA4	7.7	10.8	137.2	100.4	32.2	40.0	187.1	178.0	4.1	3.7
NB4	6.3	7.0	86.3	78.6	43.3	43.1	156.2	170.5	6.8	6.3
NA8	6.6	7.1	94.7	84.7	43.2	44.1	150.5	172.5	6.5	6.6
NB8	6.6	6.5	94.7	74.5	43.2	40.8	150.0	172.0	6.5	6.3
HA4	6.9	6.9	145.1	104.5	36.9	38.8	197.9	215.0	5.3	5.6
HB4	5.7	5.6	101.5	68.6	40.7	39.8	161.7	177.0	6.6	7.1
HA8	5.9	5.9	97.2	86.2	42.2	40.7	156.2	173.5	7.1	7.2
HB8	5.9	6.1	97.2	77.2	42.2	42.7	156.2	175.5	7.1	7.1

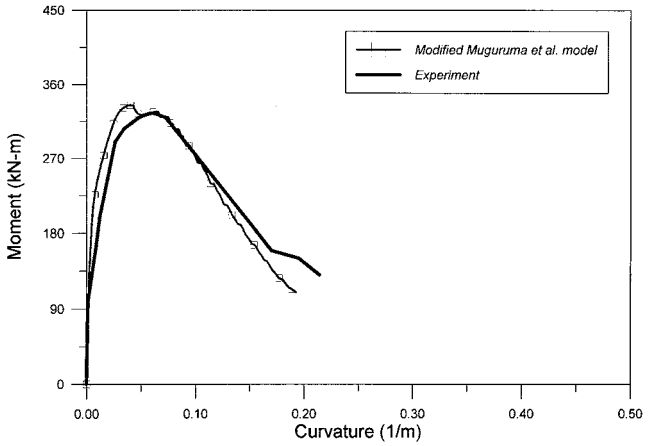

Fig. 19—Comparison of experimental results with modified Muguruma et al. model for moment-curvature curves of Specimen HB4.

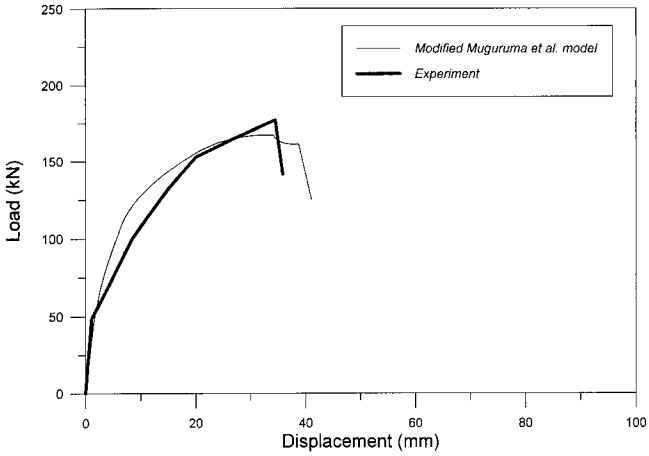

Fig. 20—Comparison of experimental results with modified Muguruma et al. model for load-displacement curves of Specimen HB4.

Comparison of experimental results with analytical model

Figure 19 shows the comparison of the modified Muguruma et al. model with the experimental results for the moment-curvature relationship of Specimen HB4. In Fig. 19, the experimental results are represented by the thick curve and the results predicted by the modified Muguruma et al. model are represented by the thin curve with square boxes. It can be seen from Fig. 19 that the moment-curvature curve predicted by the analytical model is very close to that from the tests throughout the loading history. Similarly, the lateral load-displacement relationship of Specimen HB4 using the modified Muguruma et al. model is further compared with the experimental results, as shown in Fig. 20. Note that in Fig. 20 the descending portions are plotted only until 80% of the maximum force. It can be seen from Fig. 20 that both the analytical results and test data are in good agreement. In addition, the maximum force and ductility factor are also listed in Table 5 for all eight specimens. The predicted values are also very close to the experimental results.

CONCLUSIONS

1. The stress-strain relationship of confined concrete in hollow bridge columns was determined by tests on single wall panels;

2. The analytical models of confined concrete proposed in literature could not be used to predict the stress-strain relationship of confined concrete in hollow columns tested in this study. The Muguruma et al. model was modified to fit the experimental results. It was found that the new model can well predict the stress-strain relationship of confined concrete with acceptable accuracy;

3. The spacing requirement of confining steel specified in the ACI Code could not be employed for concrete strength used in this study. In contrast, the equation suggested by Priestley, Seible, and Calvi for the spacing of confining steel can well be employed;

4. The effect of configuration of lateral steel used in this study on the stress-strain relationship of confined concrete was small and negligible;

5. When the panel test specimens are with confining steel, the ultimate strain of the specimens with normal strength (22 MPa) was approximately twice as large as that with higher strength (41 MPa);

6. The modified Muguruma et al. model can be adopted in the moment-curvature analysis to properly predict horizontal force-displacement relationship of reinforced concrete hollow columns;

7. The configuration of lateral steel used in this study has approximately a ductility factor of 6.0 when the axial force acting on the hollow column is less than $0.11f'_c A_g$;

8. Specimens with higher-strength concrete had greater ductility than those with normal strength concrete when the failure mode was reinforcing bar rupture; and

9. The failure mode may change from reinforcing bar rupture to reinforcing bar buckling if the axial force increases from 0.11 to $0.19f'_c A_g$.

ACKNOWLEDGMENTS

The research was supported by the National Science Council, Taiwan, through Research Grant NSC 87-2621-P-006-011 and the Sinotech Foundation for Research & Development of Engineering Sciences & Technologies, Taiwan. The authors wish to thank H. Y. Hung, S. H. Yao, and S. J. Wang for their assistance in construction and testing the specimens.

NOTATION

A_{ch} = area of member measured out-to-out of lateral steel
A_g = gross area of section
A_o = coefficient given in Eq. (18)
A_s = area of reinforcing bars
A_{sh} = total area of lateral steel within spacing s and perpendicular to dimension h_c
B = parameter given in Eq. (4)
B_c = width of cross section measured from centerlines of perimeter hoop
C_c = coefficient given in Eq. (17)
D_c = thickness of cross section measured from centerlines of perimeter hoop
$d_{b\ell}$ = diameter of longitudinal reinforcing bars
E_c = modulus of elasticity of concrete, given in Eq. (19)
E_s = modulus of elasticity of reinforcing bars
f_c = stress of concrete
f'_c = concrete compressive strength
f_{cc} = maximum stress of confined concrete
f_{cr} = tensile cracking strength of concrete
f_{cu} = parameter given in Eq. (15)
f_s = reinforcing bar stress
f_u = ultimate strength of longitudinal reinforcing bars
f_y = yield stress of bare reinforcing bars
f'_y = parameter given in Eq. (3)
f_{yh} = yield stress of lateral steel
$f_{y\ell}$ = yield stress of longitudinal reinforcing bars
h_c = dimension of column core measured center-to-center of confining reinforcement
P = axial force
s = spacing of lateral steel
ε = strain of concrete
ε_c = strain of concrete corresponding to f'_c as shown in Fig. 13
ε_{cc} = parameter given in Eq. (14)
ε_{cu} = strain of concrete corresponding to f_{cu} as shown in Fig. 13
ε_s = strain of reinforcing bars
ε_u = ultimate strain of unconfined concrete
ρ = ratio of area of reinforcing bars over area of concrete section
ρ_s = of lateral steel to concrete volume

REFERENCES

1. Mander, J. B.; Priestley, M. J. N.; and Park, R., "Behavior of Ductile Hollow Reinforced Concrete Columns," *Bulletin*, New Zealand National Society for Earthquake Engineering, V. 16, No. 4, Dec. 1983, pp. 273-290.

2. Taylor, A. W., and Breen, J. E., "Design Recommendations for Thin-Walled Box Piers and Pylons," *Concrete International*, V. 16, No. 12, Dec. 1994, pp. 36-41.

3. Suda, K.; Murayama, Y.; Amano, R.; and Iohinomiya, T., "Effect of Torsion on Ductility of Reinforced Concrete Piers with Hollow Section," *Proceedings of the 51st Annual Conference of JSCE*, No. 5, Sept. 1995, pp. 840-841.

4. Suda, K.; Shimbo, H.; Masukawa, J.; and Murayama, Y., "New Method for Restraint of Longitudinal Bar Buckling in Rectangular Columns with Hollow Section," *Proceedings of Technical Conference of the Great Hanshin-Awaji Earthquake*, JSCE, Tokyo, 1996, pp. 579-582.

5. Matsudal, T.; Yukawa, Y.; Yasumatsu, T.; Tsukiyama, Y.; Ishihara, S.; Suda, K.; Shimbo, H.; and Saito, H., "Seismic Model Tests of Reinforced Concrete Hollow Piers," *Proceedings of the 12th US-Japan Bridge Engineering Workshop*, 1996, pp. 407-421.

6. Suda, K.; Shimbo, H.; Masukawa, J.; and Murayama, Y., "Reinforcing Method to Improve Ductility of RC Column with Hollow Section," *Proceedings of JCI*, V. 18, No. 2, 1996, pp. 725-730.

7. Suda, K.; Amano, R.; Masukawa, J.; and Ichinomiya, T., "Effects of Torsion on Ductility of High-Piers," *Proceedings of JCI*, V. 19, No. 2, 1997, pp. 789-794.

8. Kent, D. C., and Park, R., "Flexural Members with Confined Concrete," *Journal of the Structural Division*, ASCE, V. 97, No. 7, 1971, pp. 1969-1990.

9. Muguruma, H.; Watanabe, S.; Katsuta, S.; and Tanaka, S., "A Stress-Strain Model of Confined Concrete," *Proceedings*, JCA Cement and Concrete, V. 34, Japan Cement Association, Tokyo, Japan, 1980, pp. 429-432.

10. Sheikh, S. A., and Uzumeri, S. M., "Analytical Model for Concrete Confinement in Tied Columns," *Journal of the Structural Division*, ASCE, V. 108, No. 12, 1982, pp. 2703-2722.

11. Mander, J. B.; Priestley, M. J. N.; and Park, R., "Theoretical Stress-Strain Model for Confined Concrete," *Journal of the Structural Division*, ASCE, V. 114, No. 8, 1988, pp. 1804-1826.

12. Mander, J. B.; Priestley, M. J. N.; and Park, R., "Observed Stress-Strain Behavior of Confined Concrete," *Journal of the Structural Division*, ASCE, V. 114, No. 8, 1988, pp. 1827-1849.

13. Fujii, M.; Kobayashi, K.; Miyagawa, T.; Inoue, S.; and Matsumoto, T., "A Study on the Application of a Stress-Strain Relation of Confined Concrete," *Proceedings*, JCA Cement and Concrete, V. 42, Japan Cement Association, Tokyo, Japan, 1988, pp. 311-314.

14. Saatcioglu, M., and Razvi, S. R., "Strength and Ductility of Confined Concrete," *Journal of the Structural Division*, ASCE, V. 118, No. 6, 1992, pp. 1590-1607.

15. Hoshikuma, J.; Kawashima, K.; Nagaya, K.; and Taylor, A. W., "Strain Model for Confined Reinforced Concrete in Bridge Piers," *Journal of Structural Engineering*, ASCE, V. 123, No. 5, May 1997, pp. 624-633.

16. Park, R.; Priestley, M. J. N.; and Gill, W. D. et al., "Ductility of Square-Confined Concrete Columns," *Journal of the Structural Division*, ASCE, V. 108, No. 4, 1982, pp. 929-950.

17. Sheikh, S. A., and Uzumeri, S. M., "Strength and Ductility of Tied Concrete Columns," *Journal of the Structural Division*, ASCE, V. 106, No. 5, 1980, pp. 1079-1102.

18. Razvi, S. R., and Saatcioglu, M., "Confinement of Reinforced Concrete Columns with Welded Wire Fabric," *ACI Structural Journal*, V. 86, No. 6, Nov.-Dec. 1989, pp. 615-623.

19. Muguruma, H.; Watanabe, S.; Tanaka, S.; Sakurai, K.; and Nakamura, E., "A Study on the Improvement of Bending Ultimate Strain of Concrete," *Journal of Structural Engineering*, Tokyo, Japan, V. 24, 1978, pp. 109-116.

20. Sheikh, S. A., and Khoury, S. S., "A Performance-Based Approach for the Design of Confining Steel in Tied Columns," *ACI Structural Journal*, V. 94, No. 4, July-Aug. 1997, pp. 421-431.

21. Hsu, T. T. C., *Unified Theory of Reinforced Concrete*, CRC Press, Boca Raton, Fla., 1993, 313 pp.

22. ACI Committee 318, "Building Code Requirements for Structural Concrete (ACI 318-02) and Commentary (318R-02)," American Concrete Institute, Farmington Hills, Mich., 443 pp.

23. Priestley, M. J. N.; Seible, F.; and Calvi, G. M., *Seismic Design and Retrofit of Bridges*, John Wiley & Sons, Inc., 1996, 686 pp.